ChemCatChem

Research Article
doi.org/10.1002/cctc.202301464

Chemistry Europe
European Chemical Societies Publishing

www.chemcatchem.org

Ensemble Effects on Methanol Oxidation to Formaldehyde on Ferric Molybdate Catalysts

Michael Bowker,*[a, b] Matthew House,[a] Catherine Brookes,[a, b] Pip Hellier,[a, b] and Peter Wells[b, c]

The properties of Mo-doped iron oxide are compared with those of the single oxides of Fe and Mo, and with stoichiometric ferric molybdate for the selective oxidation of methanol. It is found that Mo oxide segregates to the surface of the iron oxide at low loadings, while at higher loadings, but below the stoichiometric ratio, presents layers of ferric molybdate at the surface. The relationship between bulk loading and surface Mo is explored, and it is concluded that the reactivity is dominated by ensemble effects. Simple modelling indicates that four or more Fe cation ensembles are required to combust methanol to CO_2, ensembles of two Mo cations are required for selective oxidation to formaldehyde, whereas it seems that isolated single sites of either Fe or Mo produce CO.

Introduction

The selective oxidation of methanol to produce formaldehyde (around 24 mmt/pa in 2022)[1] is the biggest chemical use of methanol (111 mmt/annum in 2022).[2] It is thus an extremely important process and formaldehyde is used in a wide variety of products, especially in furniture manufacture as urea-formaldehyde resins.[3] Considering the new urgency for environmentally friendly ways of producing the chemicals that society needs to function, there is the possibility to make methanol, and therefore formaldehyde, in new ways. This can be by replacing environmentally damaging methane reforming to produce hydrogen with renewable energy-produced hydrogen using electrolysis or other methods. A demonstrator plant is being constructed in Sweden[4] following on from a methanol demonstrator built next to a coal-fired power station in Germany using CO_2 from that source,[5] and a number of others are in development and construction.[6–9]

One of the main catalytic routes to formaldehyde is by selective oxidation over iron molybdate catalysts,[3,10–13] and this material is the subject of this paper. We know much about the role of this material in the catalysis, but we know relatively little about the distribution of active sites, what the active surface is like at the atomic scale and the nature of those sites. Several authors have tackled this problem, coming to the overall conclusions that two adjacent Mo sites are required for the selective oxidation[13–20] and that the presence of Fe sites at the surface is detrimental to performance.

The activity of the industrial catalyst has been ascribed by many to $Fe_2(MoO_4)_3$, but there is a counter argument that MoO_3 is not simply there to replenish any lost molybdena, but it is also required for complete selectivity to formaldehyde.[21,22] MoO_3 is highly regarded for its ability to improve the selectivity of this reaction, with Bowker et al.[22] carrying out studies to show a 100% selectivity towards formaldehyde under TPD of MeOH/He. A study by Söderhjelm et al.[23] reinforces this idea that MoO_3 is not simply there to replace lost Mo. A synergistic effect between MoO_3 and $Fe_2(MoO_4)_3$ was proposed, implying that the active phase may be Mo-rich, existing as an amorphous layer in octahedral co-ordination at the surface. Each oxide was considered to play its own specific role. Specifically, MoO_3 was suggested to be there for the dissociation of molecular O_2 to atomic oxygen, whilst $Fe_2(MoO_4)_3$ utilises this atomic oxygen to oxidise methanol to formaldehyde. It was suggested that the promotion of one phase occurs at the junction of the two phases, modifying the electronic density of the catalytic active phase. This is in line with the remote control theory,[24] which was applied to catalysts with two oxide phases. $Fe_2(MoO_4)_3$ enables C–H activation, acting independently but with limited activity. MoO_3 acts as the donor phase and has a role in providing oxygen activation at a high rate, which spills over to the other phase and accelerates the overall catalytic cycle.

Here we present data and analysis regarding the distribution of these active sites at the surface by varying both the bulk loading of Mo oxide, and the surface loading into/onto an iron oxide catalyst and show that the behaviour of single and multiple iron sites is quite different from one another with the former producing CO, while the latter is the source of methanol

[a] M. Bowker, M. House, C. Brookes, P. Hellier
Max Planck-Cardiff Centre on the Fundamentals of Heterogeneous Catalysis (FUNCAT), Cardiff Catalysis Institute, School of Chemistry, Cardiff University, Cardiff CF10 3AD, UK
E-mail: bowkerm@cardiff.ac.uk
Homepage: https://www.cardiff.ac.uk/people/view/38524-bowker-mike

[b] M. Bowker, C. Brookes, P. Hellier, P. Wells
UK Catalysis Hub, RCAH, Rutherford Appleton Laboratory, Didcot OX11 0QX, UK

[c] P. Wells
School of Chemistry, University of Southampton, Southampton, SO17 1BJ, UK

Supporting information for this article is available on the WWW under https://doi.org/10.1002/cctc.202301464

combustion. It is proposed that ensemble effects dominate the surface reactivity.

Results

Fe_2O_3, MoO_3, $Fe_2(MoO_4)_3$

The catalysts made are listed in Table 1 below, with Mo:Fe ratio and molar fraction of cations.

Raman Spectra

Raman spectroscopy is a particularly useful tool for identifying which phases are present in ferric molybdate catalysts. As Figure 1 shows there are distinct bands present in the pure phase of the materials. Ferric oxide has no significant bands above 600 cm^{-1}, but a major band at 220 cm^{-1}. MoO_3 and $Fe_2(MoO_4)_3$ are distinguishable mainly by the difference in bands around 800 cm^{-1}–815 cm^{-1} for MoO_3 (Mo–O–Mo asymmetric) and 790 for $Fe_2(MoO_4)_3$ (Mo–O–Mo asymmetric). They can be further distinguished by bands just below 1000 cm^{-1} region assigned to terminal asymmetric Mo=O stretches.

Table 1. Mo:Fe ratios, molar fraction of cations and surface areas for the catalyst samples used.

Catalyst Sample	Mo:Fe ratio	Mo Molar fraction	Surface Area/m^2g^{-1}
Fe2O3	0	0	17
Mo doped Fe2O3	0.02	0.02	33
Mo doped Fe2O3	0.05	0.05	66
Mo doped Fe2O3	0.2	0.17	55
Mo doped Fe2O3	0.5	0.33	40
Mo doped Fe2O3	1.0	0.50	16
Fe2(MoO4)3	1.5	0.60	8
Super-stoichimometric	1.6	0.62	6
Super-stoichimometric	1.9	0.66	4
Super-stoichimometric	2.2	0.69	7
MoO3	–	1.0	1

XRD

X-ray diffractograms for the fundamental materials are given in the supporting information and Figure S1. The phases detected are as expected for α-Fe_2O_3, α-MoO_3 and α-$Fe_2(MoO_4)_3$.[25–27]

Methanol TPD and oxidation

Methanol TPD is an extremely useful technique for characterising these catalysts, since it is a rather direct probe of surface characteristics, being adsorbed only on the very topmost layer of the material, and it is at the surface that the catalysis with methanol takes place. Figure 2 shows the TPD data from the three fundamental materials and this reveals that iron oxide has very different behaviour to the other two materials, giving main products of combustion, CO_2, H_2O and also H_2. In contrast MoO_3 and $Fe_2(MoO_4)_3$ give only formaldehyde as a carbon product in TPD. In relation to what follows it is important to note that, within experimental error, no CO is produced.

If we then characterise these materials in an oxygen flow, the behaviour in TPD is reflected in the reactivity patterns (Figure 3). This is already given above Iron oxide produces CO at low temperatures and CO_2 at high temperatures, which also reflects its importance as a water gas shift catalyst in ammonia synthesis processes for instance. Both Mo-containing catalysts

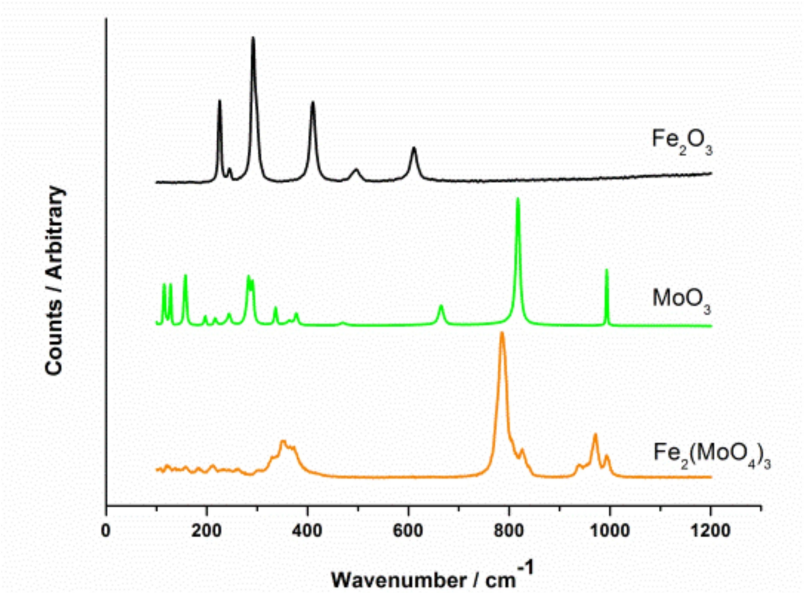

Figure 1. Raman spectra of the three stoichiometric catalysts.

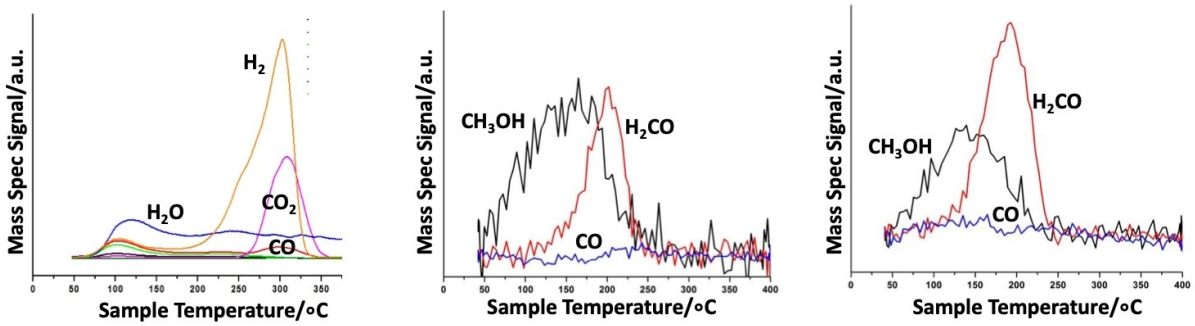

Figure 2. TPD from (left) iron oxide, (middle) MoO_3 and (right) ferric molybdate.

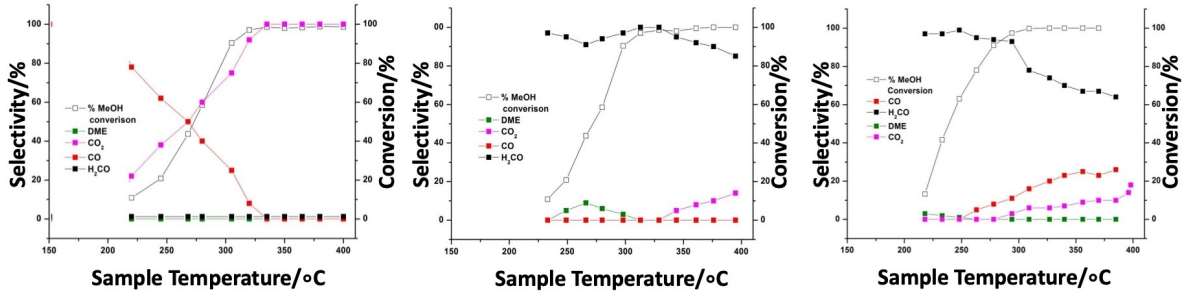

Figure 3. Reaction data for (left) Fe_2O_3, (middle) MoO_3 and (right) ferric molybdate.

are highly selective to formaldehyde, though CO/CO_2 start to appear at high temperatures. Of these the most active material is the iron molybdate, which has 50% conversion at ~230 °C, whereas it is 275 °C for both other materials. Note that that the MoO_3 has a much lower surface area than the other two, at ~1 $m^2 g^{-1}$, whereas the ferric molybdate is 6.5 $m^2 g^{-1}$ and iron oxide is 8 $m^2 g^{-1}$.

Varying the Fe:Mo ratio: Bulk Doping

To understand something about the nature of the active site at the surface of the catalyst, we have varied the stoichiometry of the catalysts, as described in the experimental section, by varying the ratio of Mo and Fe precursors in the co-precipitation process. The surface areas of these materials change significantly with the variation of Mo loading, as do some features of the precipitation process, which are described in the experimental section below. As can be seen in Figure 4 and Table 1, at very low loading of Mo the surface area is much higher than the precipitated iron oxide, which is 17 $m^2 g^{-1}$. The area of the mixed catalysts maximises at 66 $m^2 g^{-1}$ at a mol fraction of 0.05 (atomic ratio 0.05) and diminishes again after that down to 6.5 for the stoichiometric ratio of $Fe_2(MoO_4)_3$ (mol fraction 0.6) and to ~1 $m^2 g^{-1}$ for the commercial MoO_3. The very high areas seem to be related to the gel formation mentioned in the experimental section. Note that in the methanol experiments reported below, methanol was dosed in pulses to saturation before TPD, and Figure 4 shows that the trend of methanol uptake from such measurements follows the surface area variations very closely. That is, there is a linear correlation

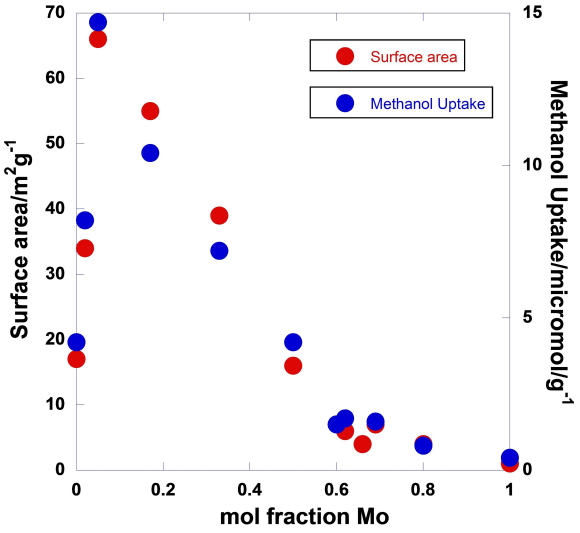

Figure 4. BET surface areas of the various catalysts made by ratio variations of Mo oxide in iron oxide compared with the uptake of methanol at 25 °C, showing that methanol uptake may be an alternative method to measure the surface area of such catalysts.

between surface area and methanol uptake, independent of the Fe:Mo ratio. Thus, methanol uptake at ambient temperature is a good way to measure oxide surface areas.

From the results presented above for iron and molybdenum oxides, and ferric molybdate, we can imagine that at low Mo levels the performance, in terms of selective oxidation, would be poor, while at high loadings it would be good, but how does it vary at intermediate doping levels? Figs. 5 and 6 show the effect in TPD and reaction measurements respectively.

In Figure 5 we can see a continuous change in the behaviour, but most noticeable perhaps is that at intermediate levels of Mo oxide, when the catalyst becomes very selective towards CO production. At a Mo:Fe ratio of 0.02 the behaviour looks essentially like that of haematite in fig 2, except for the formation of a small amount of CO at a temperature a little below that of CO_2 evolution. As the Mo loading increases so this CO desorption increases and shifts to lower temperature but then diminishes again at higher loadings. Formaldehyde begins to be seen at a ratio of 0.05, and increases with Mo loading, but always evolves at ~190 °C. The other main difference is the loss of hydrogen as Mo increases until none is seen at high loadings.

If we turn to the reactor results in an oxygen flow, these are shown in Figure 6. It has already been mentioned above Here the results in aerobic conditions are different, but parallel those in the TPD. At 0.02 ratio the material behaves very like haematite in Figure 2 this should be figure 3, except that there is now some yield of formaldehyde at low conversion/low temperature. This yield increases significantly with increasing Mo content. There is a very high yield and selectivity to CO in the intermediate loadings of Mo oxide, which then diminishes again at higher loading until formaldehyde is by far the

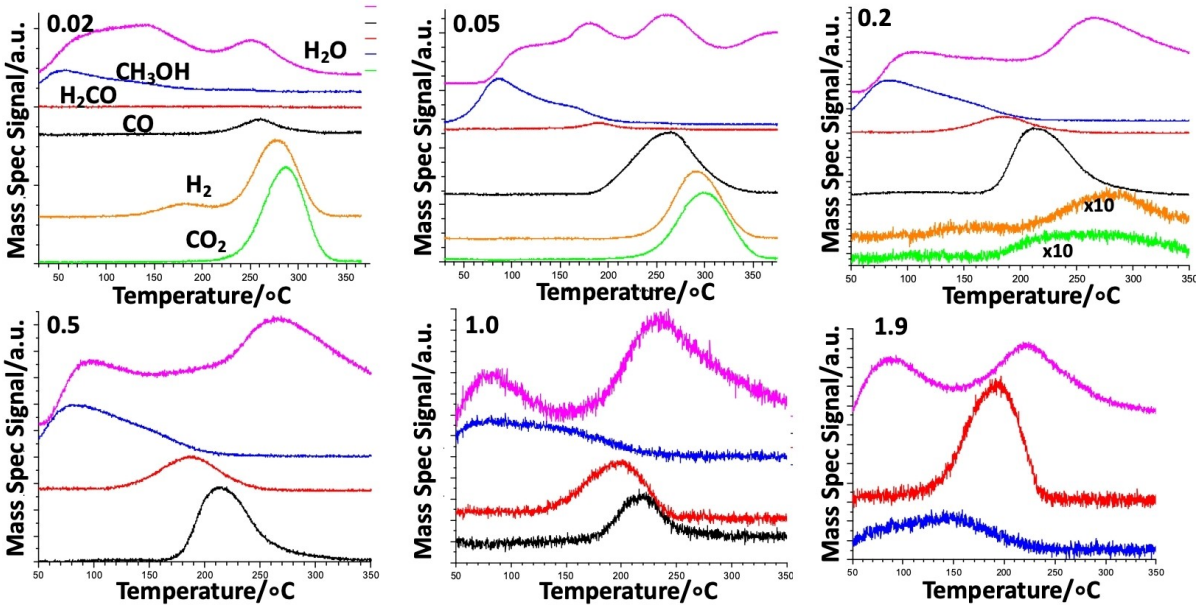

Figure 5. TPD from the various catalysts with varying Mo:Fe ratio, note that 1.6 ratio is omitted – it was essentially the same as for 1.9.

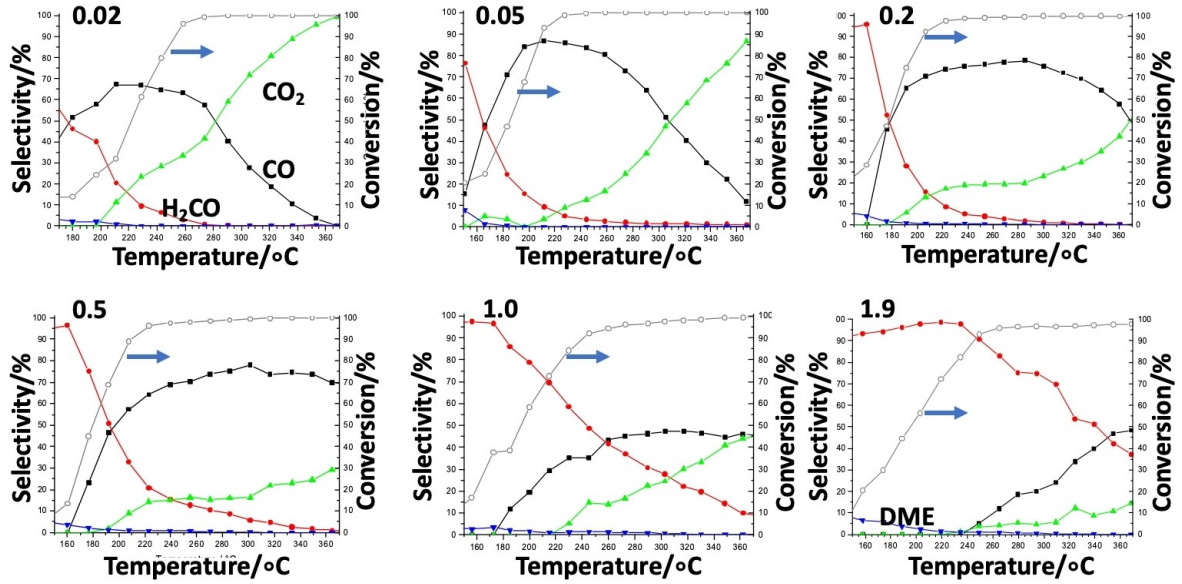

Figure 6. Selectivity and conversion dependence on temperature of reaction for the various catalysts with varying Mo:Fe ratio, note that 1.6 ratio is omitted – it was essentially the same as for 1.9.

dominant product at the super-stoichiometric Mo:Fe ratio of 1.9 (1.5 being stoichiometric for $Fe_2(MoO_4)_3$). We note that Soares et al consider that ferric molybdate is very active, but that additional molybdenum oxide is needed for high selectivity.[28] Beale et al found that ferric molybdate is produced after calcination to 400 °C from a mixed material made by hydrothermal methods.[29]

In XRD (supporting Figures S2 and S3) there is a continuous decrease in Fe_2O_3 diffraction features and increase of those from ferric molybdate in the sub-stoichiometric range of Mo doping, with the two phases of iron oxide and iron molybdate apparently co-existing. At the stoichiometric ratio of 1.5 only the ferric molybdate is seen, but above 1.6 ratio then features of MoO_3 also appear, particularly seen by the Bragg peak at 12°, evidence of the formation of crystallites of MoO_3. X-ray photoelectron (XP) spectra are shown in supporting information Figures S4 and S5 and show the presence of Mo^{6+} and Fe^{3+} states only. The XPS is discussed in more detail below. Raman spectra are shown in supporting information, Figures S6 and S7, and clearly show the presence of ferric molybdate at loadings of 0.2 and above, while there evidence of MoO_3 at ratios of 1.6 and higher.

Varying the Fe:Mo ratio: surface doping

To compare with the bulk doping method, we also doped Mo onto the surface of the catalysts by impregnation, as described in the experimental section. The results are shown for three different levels of doping in Figure 7. With 0.24 monolayers equivalent doping there was no evident formaldehyde desorption, but there was CO evolution at around 270 °C, with CO_2 at 300 °C, and hydrogen in between those. If we compare this with the bulk doping data it looks similar to that in Figure 2 for somewhere between 0.02 and 0.05 doping. At a nominal surface doping of 0.6 monolayers, then we have nearly lost the CO_2 and hydrogen, the CO has increased and shifted to ~200 °C, though the peak has a long tail to higher temperatures, and formaldehyde has appeared at ~170 °C. This looks similar to the bulk doping result at the 0.2–0.5 level. Finally, for 2.4 monolayers equivalent, the spectrum is not so different, except with more formaldehyde and a better defined, narrower, CO peak, with little tailing to high temperature, and there is no CO_2 or H_2 production. Note that an even higher doping level (7.2 monolayers) was very similar to the 2.4 monolayer result.

If we now turn to the reactor results (Figure 8), the 0.24 monolayer sample shows results similar to those for 0.02–0.05 bulk doping, that is high CO evolution at intermediate temperatures with CO_2 dominating at the highest temperature. As the surface doping goes up, so formaldehyde production increases at the expense of CO and CO_2, but CO dominates at the highest temperatures. At 7.2 monolayers the result is little different from that at 2.4. This is similar to the findings for the bulk doping level of 1.0. The 50% conversion level drops from ~220 °C at 0.24 monolayers to ~190 °C at 2.4 monolayers. This change is similar to the changes seen for bulk doping from the 0.02 to 0.2 level.

So, it seems that we have behaviour for the monolayer materials which is like that for bulk doping, but it never reaches quite the same level of high formaldehyde selectivity across the temperature range that it does for bulk doping when the latter is at/above the stoichiometric level for $Fe_2(MoO_4)_3$.

In XRD it was very difficult to see any bands due to ferric molybdate because of the low amount of Mo dosed, which presumably results in a thin/amorphous layer of material. However, Raman bands for ferric molybdate can be seen for a 3

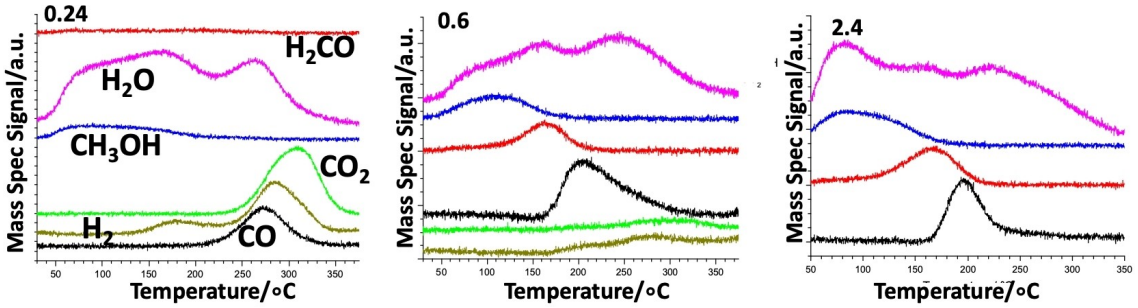

Figure 7. TPD after dosing methanol at ambient temperature on monolayer dosed Fe_2O_3: left 0.24, middle 0.6 and right 2.4 monolayers equivalent of Mo.

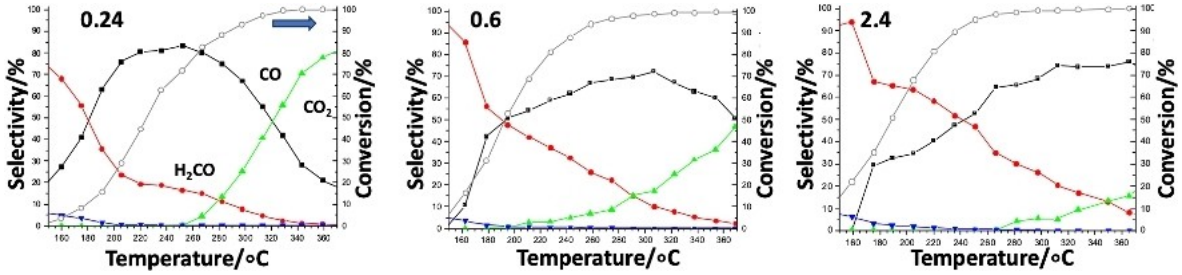

Figure 8. Reactivity profiles for the surface doped materials with 0.24, 0.6 and 2.4 monolayers of Mo dosed onto the surface.

monolayer sample after calcination.[19,20] XP spectra show all samples to be in the +3 oxidation state for Fe and +6 for Mo, examples are given in the supporting information, Figures S8 and S9.

Discussion

The surface of the catalysts

It is quite clear from the data that even relatively small amounts of Mo, certainly by 0.05 Mo:Fe ratio and by 0.24 monolayer surface doping of Fe_2O_3, that there is already a significant effect on the reactivity pattern, with CO and formaldehyde beginning to appear in the reactivity profile. Table 2 gives estimates of what the Mo coverage on the surface would be for the cases where it is present as layers of stoichiometric $Fe_2(MoO_4)_3$, further description of these estimates is given in the supporting information. Note that in XPS all the catalysts made have Mo in the +6 and Fe in the +3 oxidation states (see supporting information and Figures S4,5 and 8,9). Table 3 shows data for the Mo level in the *surface region* estimated from XPS analysis of these catalysts. The *surface region* is not the surface layer itself since the escape depth (or inelastic mean free path, IMFP) indicates that a number of surface layers are probed (IMFPs for Mo and Fe oxides are not so different at ~2 nm, see supporting information). We have estimated the number layers of MoO_3 or layers of $Fe_2(MoO_4)_3$, assuming they are located at the surface only. We can immediately eliminate the former, since in that case, at high levels of doping i) we would see very little Fe signal in XPS (which, as shown below in Table 3, is not the case) and ii) the TPD (Figure 5) and reactor results (Figure 6) would be like MoO_3 and they are not, since CO is still seen. It is evident from Table 3 that there is much more Mo oxide in the surface region than expected for the dosed ratio, since the XPS ratio found is much higher than the bulk ratio up to ~0.5 Mo:Fe ratio.. It is around three to four times that which might be expected for a randomised level of Mo at the bulk ratio for the lowest two amounts of Mo. This enhanced ratio can be seen up to around 0.2, but by a ratio of 0.5 the XPS indicates ratios similar to that in the bulk, and the stoichiometric ratio material shows that ratio in XPS. What can be seen from Table 2 is that by 1.0 doping we may expect little change in the XPS signal with further Mo addition up to the stoichiometric ratio, since those layers are already significantly thicker than the IMFP and are probably iron molybdate-like. There is some discrepancy at those ratios (0.5 and 1) from what we can expect from the model in Table 2. The exact reason from this may be that the iron molybdate layers below the topmost layer(s) have a higher level of Fe than from the simple model of Table 1. Maybe the distribution is not a step function between stoichiometric ferric molybdate and iron oxide, but that there is more of a gradual variation of Mo level from the high level at the surface to the zero level for pure iron oxide. Nevertheless, at low loadings there is significant segregation of Mo oxide to the surface region.

There is still a significant Fe signal at high loadings and at a ratio of 1.5 has values close to that expected for the stoichiometric material (Table 3); at higher loadings it increases

Table 3. XPS results for the various catalysts, with the determined surface mol fraction of Mo: the final column shows that expected for Mo if segregated to the surface as iron molybdate.

Catalyst composition	XPS ratio	Expected ratio from Table 2
Fe2O3	0.00	0.0
Mo:Fe 0.02	0.09	0.07
Mo:Fe 0.05	0.15	0.11
Mo:Fe 0.2	0.44	0.53
Mo:Fe 0.5	0.55	0.93
Mo:Fe 1.0	1.01	1.5
Mo:Fe 1.5	1.55	1.5
Mo:Fe 2.2	2.2	*

* the expected ratio is uncertain since there is now extra MoO_3 at the surface, both as monolayers(s) and nanoparticles above that expected for the stoichiometric ratio.

Table 2. Estimates of surface coverage of the catalysts by Mo if segregation as ferric molybdate is assumed complete.

Catalyst Mo:Fe ratio	Surface Area/m^2g^{-1}	Average Particle radius/nm*	Approximate Number of Layers	Approximate Surface Mo monolayers as $Fe_2(MoO_4)_3$
Fe2O3 0.00	17	33	100	0
Mo:Fe 0.02	33	16	48	0.5
Mo:Fe 0.05	66	8	24	0.8
Mo:Fe 0.20	55	10	30	4.0
Mo:Fe 0.5	40	13	39	12
Mo:Fe 1.0	16	35	106	70
Mo:Fe 1.5	8	66	200	200
Mo:Fe 2.2	7	75	227	excess Mo
Mo:Fe 4.0	4	150	450	excess Mo

*calculated from the specific surface area SA/W as $r = 3/\rho SA$, where r is in m, ρ is in g/m^3 and W is in g.

a little probably due to the presence of MoO_3 in the surface of the catalyst. The evidence for its presence at above a ratio of 1.5 is given in the supporting information (Figure S7, seen in Raman by the appearance of the 290, 660, 820 and 998 cm^{-1} bands typical of MoO_3 and likewise the diffraction features in XRD at 12, 27 and 38°[16] (Figure S3, at 2.2 ratio).

The active sites

If we consider a simple model of how the surface behaves, we can imagine the surface lattice as in Figure 9. What we know from the above data is that Mo has a drastic effect on the behaviour of the iron oxide even at low loadings, when we would imagine that there are isolated sites of Mo on the surface (Figure 9, left hand). We also know that at these loadings the main new effect is to produce CO. As we go to intermediate loadings of Mo oxide, such as might be the case in the middle diagram of Figure 9, then CO is maximised and there is now very little CO_2, but there is significant formaldehyde production, and finally in the situation of the right-hand side of fig 9 there is high selectivity to formaldehyde. From those results we can infer the following:

i) isolated Mo sites produce CO (isolated sites of Fe probably also);
ii) ensembles of Fe are required to produce CO_2 (since this product dramatically falls even at low loadings of Mo)
iii) two or more Mo oxide sites are required for formaldehyde production, as already proposed by several authors,[14–20] and hence why it is maximised at high loadings.

The distribution of such sites can be described in a simple manner, with a randomised distribution of sites, by the following binomial relationship. We can then test how well such a model fits the data –

Dual surface site occupation by Fe	Fe–Fe=N_{Fe}^2
Dual surface site occupation by Mo	Mo–Mo=N_{Mo}^2
Single surface isolated site occupation by	FeMo = 1-(Fe–Fe)-(Mo–Mo) Fe or Mo

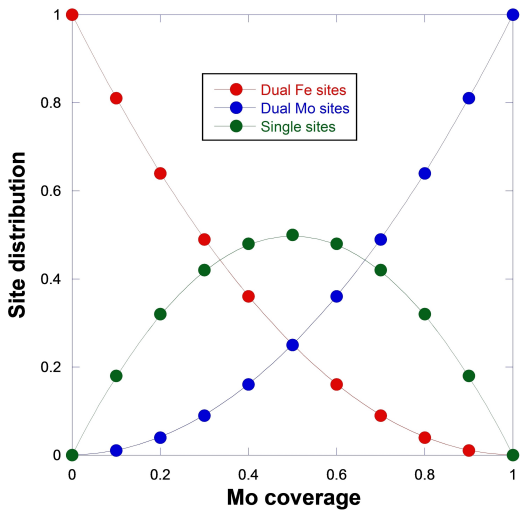

Figure 10. The distribution of sites on the surface by the simple ensemble method.

where, N_{Fe} is the fractional the number of Fe sites, N_{Mo} is the Mo sites and $N_{Fe}+N_{Mo}=1$. This then has the form shown in Figure 10, which shows a symmetric distribution of sites as the Mo coverage increases. If we now examine how the real system behaves, we show the data in Figure 11, and this seems to show broadly similar features. That is, CO_2 diminishes fast at low loadings of Mo, formaldehyde increases at high loadings and in between these CO shows a maximum of production. This production is very high at intermediate loadings. Of course, the bulk loading is not the surface loading, but as we've seen from the XPS above, there is certainly segregation of Mo oxide to the surface region of the catalysts, especially enhanced (in terms of increased amount with respect to that expected from the loading level) at ratios up to ~0.2. To try to correlate bulk loadings with surface Mo, the surface doping values have been placed onto Figure 11 at the points where the selectivity agrees reasonably well with the bulk loading results. As can be seen from the figure 0.24 monolayers of Mo dosed at the surface corresponds with around 0.03 bulk Mo:Fe ratio, while 0.6 monolayers is equivalent to 0.7 and 2.4 monolayers approximates to 1.2 ratio. So, it is clear that there is an initial significant segregation of Mo oxide into the surface layer(s) of the material,

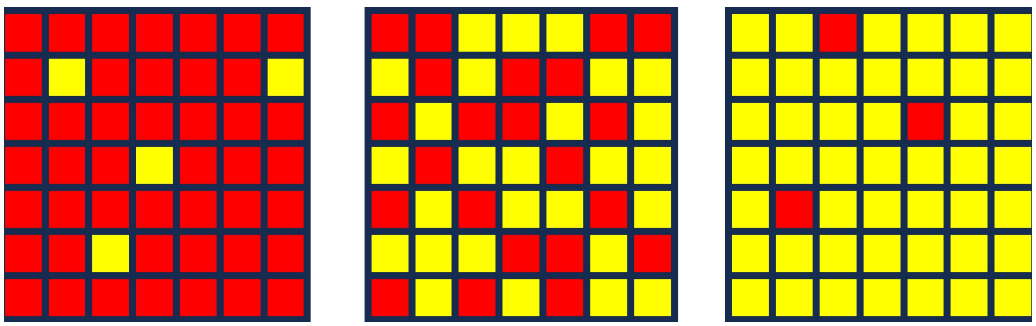

Figure 9. Schematic diagram of randomised site distribution with Fe as red sites and Mo as yellow. The left hand diagram is for a surface dilute in Mo, with the centre diagram at roughly 50% coverage with Mo, while the right hand represent a surface mostly covered in Mo sites.

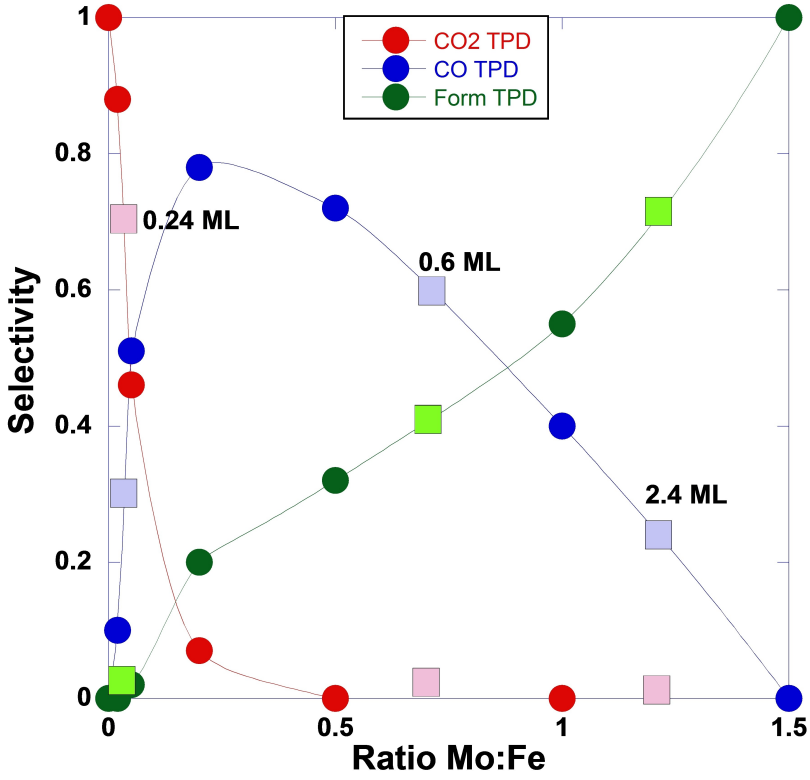

Figure 11. Product selectivity from TPD dependence on Mo:Fe ratio from the experiments described above (circles). The data for selectivity from the monolayer (ML) dosing TPD experiments (squares) are placed on this plot where the selectivities for the surface and bulk loadings agree to give an idea of the surface Mo level for the similar selectivity bulk loading. For surface doping data: pink squares, CO_2; pale blue CO; pale green H_2CO.

which especially affects the amount of CO_2 produced, but that as the loading goes up the effect, though still there, is reduced. As stated above 7.2 monolayers dosed is little different from 2.4 monolayers. So, by that method of dosing we never get to the very high selectivity achieved by bulk dosing to high Mo levels and by industrial catalysts.

All of this indicates that, although there is considerable preferential segregation of Mo oxide into the surface region of the Fe, the surface is not completely stoichiometric. Indeed, even at 7.2 monolayers dosed, the behaviour is very similar to that for 2.4 monolayers. This implies that we never reach the very high selectivity of the stoichiometric material, $Fe_2(MoO_4)_3$ (as in figures 5 and 6), by the surface doping method, and that there are isolated sites left of the type which produce CO. It is probably because the surface is ferric molybdate-like, with roughly 40% of the sites being Fe^{3+}, so with a selectivity not far from that suggested by Figure 10. In fact, we and others proposed earlier[17,19,30] that there is extra Mo at the surface of the selective ferric molybdate catalyst and that this is by far the most selective material. It is likely to be a monolayer on top of the ferric molybdate and it is to be noted that industrial catalysts have extra Mo above the stoichiometric material, often as high as 2.2:1 Mo:Fe ratio. The role of this extra Mo is also to maintain the surface MoOx layer intact, due to loss of Mo which occurs during catalyst life onstream.[31–33]

The data in Figure 11 were from TPD under anaerobic conditions (He flow). If we now turn to the data under oxygen flow conditions, in Figure 12 we show the effects of varying the ratio on the products in the catalytic reaction in oxygen. Again, the results are broadly similar to those from TPD, that is, there is a big effect of low loadings of Mo on selectivity to CO_2 and CO is the main product of the reaction. At intermediate ratios, formaldehyde starts to dominate, at the expense of CO and finally with high Mo levels, the catalyst has 96% selectivity to formaldehyde at 50% conversion. Again, on the figure we have tried to equate the results for the surface loading by placing them at points of the same selectivity for formaldehyde and these then also agree well with the selectivity of the other two products. The behaviour implies that 0.24 monolayers surface doping is equivalent to around 0.05 mol fraction bulk doping and 0.6 monolayers surface doping is equivalent to about 0.2. This further implies that low bulk loadings of Mo oxide tend to segregate to the surface region.[33] However, loadings of more than a monolayer equivalent of Mo do not correspond with the very high selectivity levels that might be expected if it were solely Mo at the surface in Figure 10, presumably because the surface is ferric molybdate-like, with Fe present in the surface layers, and not a complete layer of Mo at the surface.

Comparing the results from the two methods, anaerobic TPD and aerobic reactor data, although conducted under such different conditions, the two sets show the same general trends with the dramatic effects on CO_2 selectivity at low Mo, high formaldehyde selectivity at high Mo, and maxima in CO selectivity at a similar value, ~0.75 or 75%.

Research Article
doi.org/10.1002/cctc.202301464
Chemistry Europe
European Chemical Societies Publishing

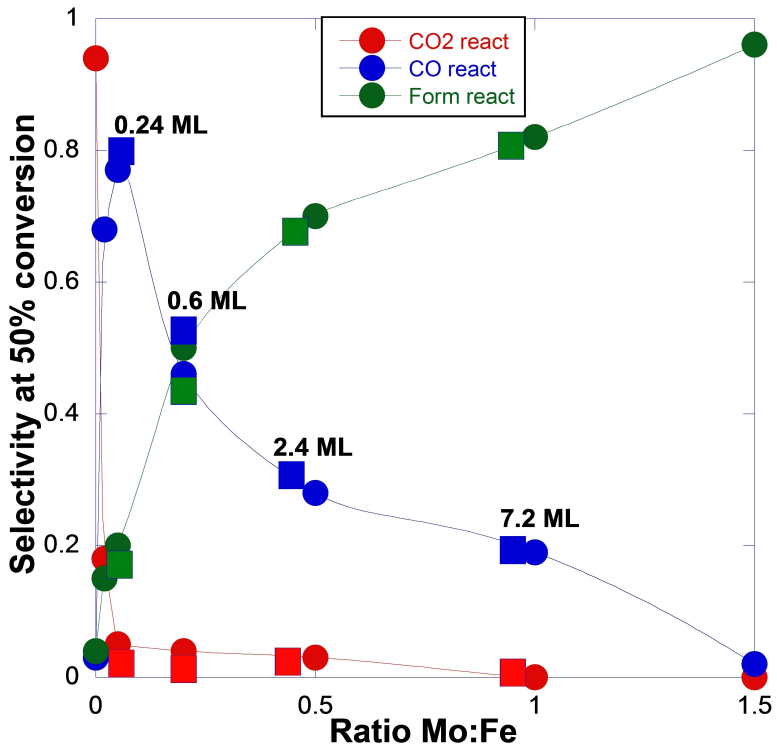

Figure 12. The dependence of selectivity, measured at 50% conversion upon the mol fraction of Mo. The numbers from the surface doping of Mo are placed on the figure to indicate where the results agree with the bulk doping values.

What is clear from both surface analysis and reaction results, is that Mo in the surface region has, as might be expected, dramatic effects on reactivity, knocking out CO_2 production at low surface levels, and producing formaldehyde at high surface levels. Hence Fe is the source of CO_2 and Mo the source of formaldehyde, but intermediate Mo oxide coverage behaviour is very different, producing CO also, with very high selectivity to this product at 0.24–0.6 monolayers dosed onto the surface. The behaviour is broadly similar to that described by the simple ensemble theory in figures 9 and 10, except that the effect on CO_2 is especially marked in both cases, with little production at even 0.2 ratio. The effect in the reactor in the presence of oxygen is more severe on CO_2 production than it is in TPD, and although the peak selectivity of CO is similar, it is skewed to much lower loadings for the reactor data. Direct comparison of the latter is difficult since i) only 50% conversion data was chosen for comparison and ii) the temperature for 50% conversion varies, as can be seen in Figure 6. Nonetheless Table 4 shows the comparison of the points in Figure 11 where the selectivity values for surface and bulk doping agree, and again these show that at low loadings there is preferential segregation of Mo oxide.[33,34] Note that after 0.6 monolayers surface doping there not much change in the TPD, implying that the surface monolayer of ferric molybdate is near complete, as might be expected from that amount, the stoichiometric amount of Mo. In turn this implies that the Mo stays in the surface layers when dosed there, even at low levels.

The effect of Mo at the surface upon CO_2 production seems greater than might be expected from Figure 10. The oxygen demand for the combustion requires three times as much oxygen as does the selective reaction, so it may be that a bigger ensemble of Fe–O sites is required. If instead of modelling dual sites of Fe, we model a higher number then the result is shown in Figure 13. If we imagine that for every O atom removed, we need two Fe atoms to be converted to Fe^{2+}, then six would need to be converted in burning one methanol molecule. As can be seen in Figure 13, the effect of increasing the ensemble size is i) to shift the maximum in single sites to

Table 4. Comparison of bulk doping with surface doping at points in Figure 11 where catalytic performance is similar and with Table 3 for approximate XPS ratio at that point.

Surface doping level/monolayers	Bulk sample ratio Mo:Fe	XPS Mo:Fe ratio for surface doping	XPS Mo:Fe ratio for bulk doping
0	0	0	0
0.24	0.03	0.15	~0.11
0.60	0.7	0.48	~1

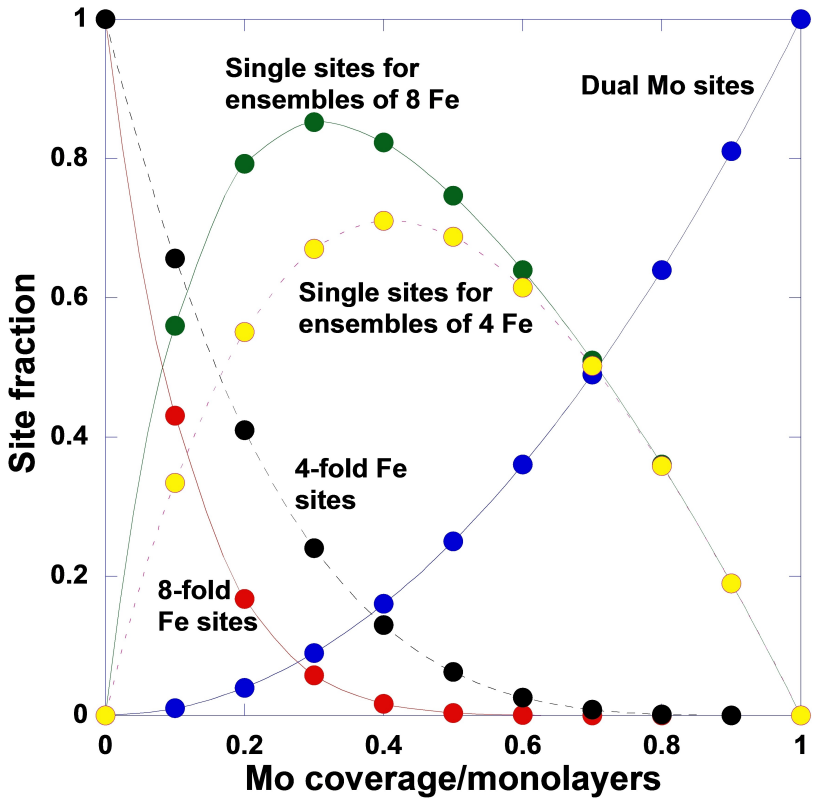

Figure 13. As for Figure 10, but here considering that quadruplet and octuplet Fe site ensembles are required for combustion of methanol.

lower Mo coverage, ii) to increase the fraction of single sites at the peak and iii) to reduce the number of active ensembles of Fe to lower Mo loadings than in Figure 10. In fact, it is remarkable that the maximum fraction of single sites we observe in Figure 11 is about the right value for a requirement for the use of three oxygen atoms (from an ensemble of six Fe ions), and at a molybdenum coverage between 0.3–0.4, and from Table 2 and Figure 11, at a bulk ratio of ~0.2.

It is interesting that the surface loading process does not achieve very high selectivity to formaldehyde. This is a reflection of the fact that such a method produces near-stoichiometric surface layers of $Fe_2(MoO_4)_3$ and the selectivity of that material is ~70% (Figure 11, 2.4 monolayers dosed) because the surface is not covered with Mo, but has ~40% of the cations as Fe. Regarding Figure 13 it corresponds with rather a higher coverage point of 0.8 monolayers of Mo. Very high selectivity near 100% is only achieved if the surface is completely covered by Mo, which only occurs by making the catalyst with Mo:Fe ratios ~ > 1.5.

A schematic model summarising this behaviour is as shown in Figure 14, with iron-rich regions combusting methanol, molybdenum-rich regions carrying out the selective reaction to formaldehyde, and mixed regions producing mainly CO. The nature of the materials that have been produced by surface and bulk doping methods is illustrated in Figure 15. Here, with surface doping, Figure 15a, the Mo oxide remains segregated mostly in the surface region, and once multi-monolayer levels have been dosed, ferric molybdate is formed in the surface region, which is selective, but not as selective as the industrial type of catalyst. Figure 15b shows the effect of doping the bulk of mainly iron oxide-based catalysts by coprecipitation with molybdenum. Here again there is movement of Mo oxide to the surface, so that at low levels of doping, even as low as 0.05 Mo:Fe ratio, there is a dramatic effect on selectivity (figures 11 and 12). Again, higher levels approach an iron molybdate-like surface layer, with good selectivity to formaldehyde, but not as good as for the material in Figure 15c. Here the bulk has been saturated with the stoichiometric amount of Mo to make ferric molybdate, $Fe_2(MoO_4)_3$, and extra Mo coats the surface in a layer without any iron present; this is the nature of the industrial type of catalyst with very high selectivity to formaldehyde. The latter usually has a lot of extra Mo, often having super-stoichiometric levels of Mo well above that needed for ferric molybdate, which has bulk-like MoO_3 present in the form of nanoparticles, here shown covering parts of the surface, in a Stranski-Krastanov-like growth mode. This is needed to compensate for loss of Mo through volatilisation during running.[31–34] We note that this model of Figure 15 has similarities with that proposed by Huang et al[18] for materials produced by a very different method, that is, by mechanical grinding of iron oxide and molybdenum oxide. There they find "thermal spreading" of the molybdenum oxide over the iron oxide, and the exact nature of the surface layers formed then depend on the calcination temperature. At our temperature of calcination (500 °C) they find a maximum in Mo in the surface region.

Research Article
doi.org/10.1002/cctc.202301464
Chemistry Europe
European Chemical Societies Publishing

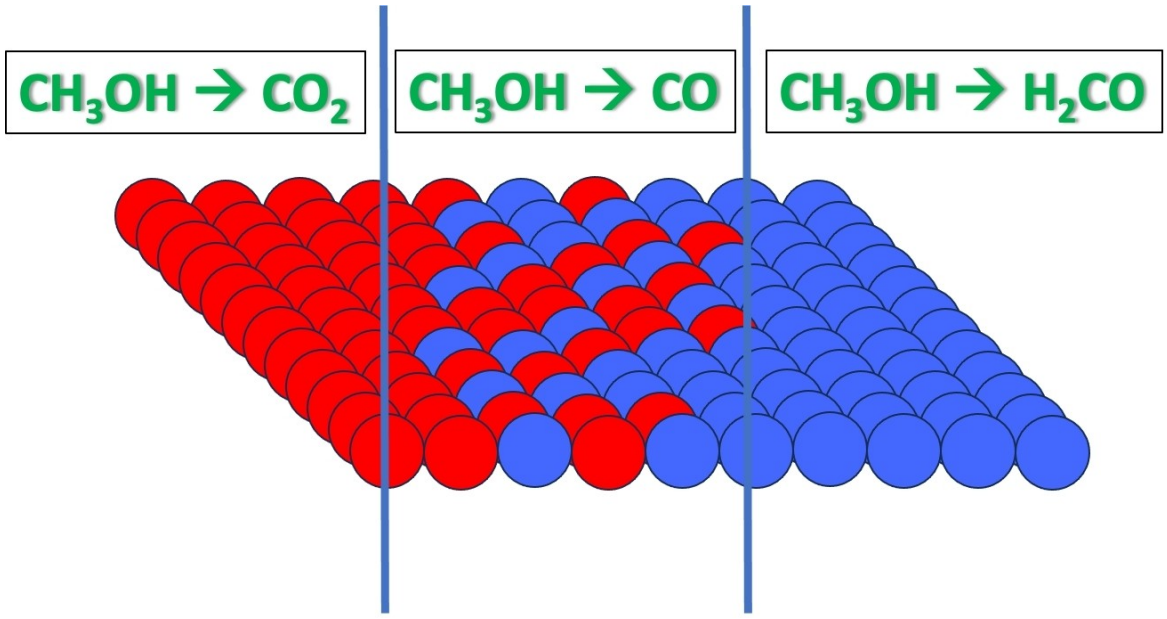

Figure 14. A schematic illustration of the roles of different sites in giving different products from methanol oxidation. On the left of the figure pure Fe site ensembles combust methanol, while on the right pure Mo site ensembles selectively oxidise methanol to formaldehyde. In the middle region there are many isolated sites of Fe and Mo which produce CO.

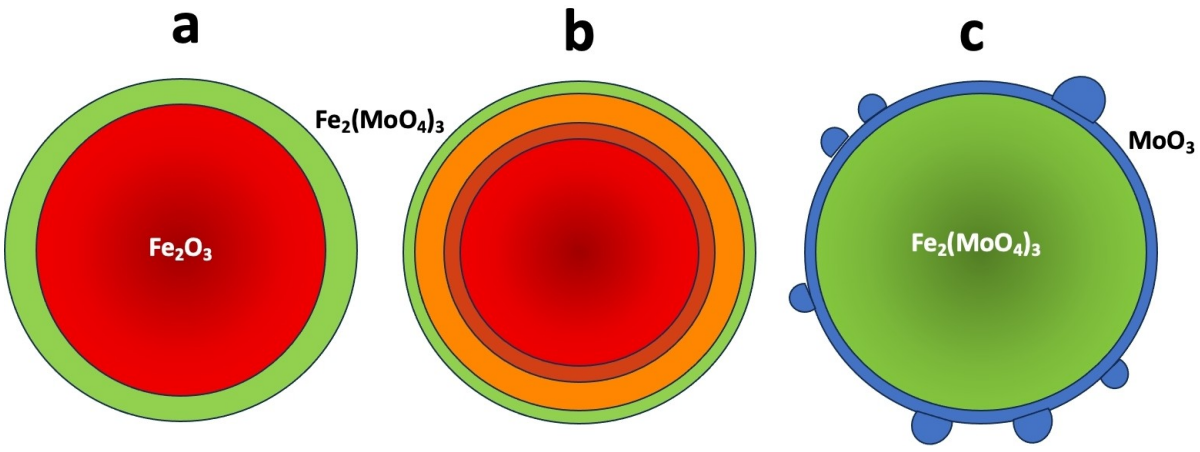

Figure 15. A schematic illustration of the effects of Mo doping into/onto iron oxide. a) Surface doping creates Mo-rich layers, which increase from low doping as individual sites of Mo at the surface to higher levels and eventually, above 0.6 monolayers ferric molybdate-like layers localised in the surface region. b) bulk doping results in Mo oxide segregation to the surface region and formation of ferric molydate-like surface layers over the iron oxide core. It is likely that there is a gradation from the surface layer of high Mo concentration to low in the core iron oxide. c) eventually if bulk doping continues to the stoichiometric ferric molybdate material and higher Mo levels, a molybdenum oxide layer forms at the surface and super-stoichiometric ratios also have extra molybdenum oxide particles.

We might ask ourselves why Fe is used at all in such materials, since it's presence at the surface results in low selectivity to formaldehyde. There are probably a number of reasons for this, including that it is a cheap, earth-abundant material and that it appears to provide a good support base for the molybdenum oxide over layer and that it provides for a higher surface area form of MoO_3. Others have suggested that there could be better catalysts. For instance, Thrane et al[35] consider that apatite may be a more stable and active support medium for molybdenum oxide, and Bowker et al[36] report that higher area, more active materials may be produced by Al doping in the bulk of the catalyst.

Experimental

The catalysts were made in the following way. Catalysts with varying bulk ratios of molybdenum to iron were created using the method of co-precipitation, followed by evaporation to dryness. The desired amount of ammonium heptamolybdate ($(NH_4)_6Mo_7O_{24}.4H_2O$, BDH, 99%) was dissolved in 100 ml deionised water before being acidified to ~pH 2 using nitric acid (HNO_3, Fisher, Laboratory Grade). To this a solution of iron nitrate (Fe(NO3)3.9H2O, BDH, 98%, 6.83 g in 50 ml) was added dropwise with stirring at 60 °C. A precipitate was formed, which was evaporated to near dryness at 90 °C. The resulting solids were dried at 120 °C overnight before being calcined to 500 °C for 48 hours. The addition of the iron nitrate initially lead to the precipitation of

a canary yellow precipitate, but with ratios lower than 1.5:1 Mo:Fe, this precipitate dissolved, before a dark brown gel was formed in the bottom of the crucible while the water was evaporated. Evaporation was carried out to near dryness at 90 °C. The resulting solids were dried at 120 °C overnight before being calcined to 500 °C for 48 hours.

In addition to catalysts with varying bulk ratios, catalysts with molybdenum dosed onto the surface of iron oxide were also created. In calculating the loading to add, it was assumed that a surface of Fe_2O_3 contains 10^{19} surface sites m^{-2}, with a total of 5/12 of these being metal cations since it was thought a $Fe_2(MoO_4)_3$ layer may form. This corresponds reasonably well with the value previously reported for MoO_3 spreading on Fe_2O_3, which showed ~70% coverage at ~6 nm^{-2} (i.e. complete coverage as ferric molybdate would correspond to about 4×10^{18} surface cations m^{-2}).[18] The sample of Fe_2O_3 used for this was created in house by the dropwise addition of 50 ml iron nitrate (Fe(NO3)3.9H2O, BDH, >98%) solution, to a dilute solution of 100 ml nitric acid (~pH 2, HNO_3, Fisher, Laboratory Grade) with stirring at 60 °C. Water was then evaporated from the sample at 90 °C, before overnight drying at 120 °C and calcination at 500 °C for 48 hours. The monolayer catalysts were then made by the incipient wetness method of impregnation onto a synthesised Fe_2O_3 with a surface area of 11.8 $m^2 g^{-1}$. The appropriate amount of ammonium heptamolybdate for the Mo surface loading, calculated as above, was made into an aqueous solution and added to iron oxide until the pores of the support were full. The material was then dried overnight at 120 °C. Calcination of the material was carried in-situ in 10% O_2/He gas flow after loading to the reactor at 400 °C for 30 minutes. Catalysts were made with nominally 24, 60, 240 and 720% ML (0.28, 0.70, 2.8 and 8.5 w/t%) of MoO_3

The experiments were carried out using a pulsed flow microreactor. That instrument can carry out temperature programmed desorption (TPD) in a He flow after dosing the adsorbate (in this case methanol). It can also be run in either continuous flow mode or pulsed flow mode, as used in this work, with a variety of gases flowing, but in this case with pulses of methanol into a continuous flow of 10%O_2/He. Surface areas were measured by the BET method with a Micromeretics Gemini 2360 instrument. The XRD spectra were obtained using a Enraf Nonus FR590 fitted with a hemispherical analyser. The conditions employed were Cu Ka radiation with a voltage of 40 kV and a current of 30 mA.

XPS measurements were made with a Kratos AXIS (DLD) fitted with a monochromated Al Ka radiation source and a refocusing lens to give high resolution XPS. The survey scans were acquired with a pass energy of 160 eV in a single sweep with a step of 0.5 eV. Region scans were acquired with a pass energy of 40 eV, in 5 to 10 sweeps in steps of 0.1 eV. Raman spectroscopy utilised a Renishaw Ramascope, which was operated by placing a small amount of sample (~0.1 g) on an aluminium slide and a laser to focus on the sample using a camera linked to the controlling computer. The spectra were then be recorded using the green argon ion laser (514 nm), with an output of less than 30 mW.

Supporting Information

The authors would like to acknowledge the UK Catalysis Hub, funded through EPSRC Grants EP/R026939/1 and EP/R026815/1, and for EPSRC EP/S030468/1 and for studentships to MH, CB and PH. We thank the Max Planck Society and Cardiff University for financial support to create the FUNCAT Centre.

Acknowledgements

Further information regarding XRD, XPS and Raman data is given in the supporting information together with additional references [37–40].

Conflict of Interests

The authors declare no conflict of interest.

Data Availability Statement

The data that support the findings of this study are available in the supplementary material of this article.

Keywords: Ensembles · formaldehyde · iron molybdate catalysts · methanol · methanol oxidation

[1] https://www.chemanalyst.com/industry-report/formaldehyde-market-627#, accessed 19 Sept 2023.
[2] https://www.statista.com/statistics/1323406/methanol-production-worldwide/accessed 19 Sept 2023.
[3] H. I. Mahdi, N. N. Ramlee, D. H. da Silva Santos, D. A. Giannakoudakis, L. H. de Oliveira, R. Selvasembian, N. I. Wan Azelee, A. Bazargan, L. Meili, *Molecular Catalysis* **2023**, *537*, 112944.
[4] https://www.carbonrecycling.is/circlenergy-news-1/2019/12/16/related-project-fresme-sfdtyNn.
[5] https://www.aspire2050.eu/mefco2.
[6] A. Jahsi, https://www.thechemicalengineer.com/news/consortium-develops-power-to-methanol-demonstration-project/.
[7] J. M. Voß, T. Daun, C. Geitner, S. Schluter, T. Schulzk, *Chem. Ing. Tech.* **2022**, *94*, 1489–1500.
[8] https://renewable-carbon.eu/news/successful-demonstration-of-methanol-production/accessed 19 Sept 2023.
[9] https://matthey.com/project-air.
[10] A. P. V. Soares, M. F. Portela, A. Kiennemann, *Catal. Rev.* **2005**, *47*, 125–174.
[11] M. I. Malik, N. Abatzoglou, I. E. Achouri, *Catalysts* **2021**, *11*, 893.
[12] R. N. Hader, R. D. Wallace, R. W. McKinney, *Ind. Eng. Chem.* **2002**, *44*, 1508–1518.
[13] J. Thrane, U. V. Mentzel, M. Thorhauge, M. Høj, A. D. Jensen, *Catalysts* **2021**, *11*, 1329.
[14] J. N. Allison, W. A. Goddard III, *J. Catal.* **1985**, *92*, 127.
[15] H. Yamada, M. Niwa, Y. Murakami, *Appl. Catal. A* **1993**, *96*, 113.
[16] T. Waters, R. A. O'Hair, A. G. Wedd, *J. Am. Chem. Soc.* **2003**, *125*, 3384–3396.
[17] M. P. House, A. F. Carley, R. Echeverria-Valda, M. Bowker, *J. Phys. Chem. C* **2008**, *112*, 4333–4341.
[18] Y. Huang, L. Cong, J. Yu, P. Eloy, P. Ruiz, *J. Mol. Catal. A* **2009**, *302*, 48–53.
[19] C. Brookes, P. P. Wells, G. Cibin, N. Dimitratos, W. Jones, M. Bowker, *ACS Catal.* **2014**, *4*, 243–250.
[20] C. Brookes, M. Bowker, P. P. Wells, *Catalysts* **2016**, *6*, 92.
[21] M. Bowker, R. Holroyd, A. Elliott, A. Alouche, C. Entwistle, A. Toerncrona, *Catal. Lett.* **2002**, *83*, 165–176.
[22] M. P. House, A. F. Carley, R. Echeverria-Valda, M. Bowker, *J. Phys. Chem. C* **2008**, *112*, 4333–4341.
[23] E. Söderhjelm, M. P. House, N. Cruise, J. Holmberg, M. Bowker, J.-O. Bovin, A. Andersson, *Top. Catal.* **2008**, *50*, 145–155.
[24] I. E. Wachs, K. Routray, *ACS Catal.* **2012**, *2*, 1235–1246.
[25] JCPDS Card Number 35–659.
[26] JCPDS Card Number 33–664.
[27] JCPDS Card Number 31–642.
[28] A. P. V. Soares, M. Farinha Portela, A. Kiennemann, L. Hilaire, J. M. M. Millet, *Appl. Catal. A* **2001**, *206*, 221–229.

[29] A. M. Beale, S. D. M. Jacques, E. Sacaliuc-Parvalescu, M. G. O'Brien, P. Barnes, B. M. Weckhuysen, *Appl. Catal. A* **2009**, *363*, 143–152.
[30] K. Routray, W. Zhou, C. J. Kiely, W. Grünert, I. E. Wachs, *J. Catal.* **2010**, *275*, 84–98.
[31] B. I. Popov, V. N. Bibin, G. K. Boreskov, *Kinet. Katal.* **1976**, *17*, 371–377.
[32] A. Andersson, M. Hernelind, O. Augustsson, *Catal. Today* **2006**, *112*, 40–44.
[33] K. V. Raun, L. F. Lundegaard, J. Chevallier, P. Beato, C. C. Appel, K. Nielsen, M. Thorhauge, A. D. Jensen, M. Høj, *Catalysis Science, Technology* **2018**, *8*, 4626–4637.
[34] K. V. Raun, L. F. Lundegaard, P. Beato, C. C. Appel, K. Nielsen, M. Thorhauge, M. Schumann, A. D. Jensen, J.-D. Grunwaldt, M. Høj, *Catal. Lett.* **2020**, *150*, 1434–1444.
[35] J. Thrane, C. Falholt Elvebakken, M. Juelsholt, T. L. Christiansen, K. M. Jensen, L. P. Hansen, L. F. Lundegaard, U. V. Mentzel, M. Thorhauge, A. Degn Jensen, M. Høj, *ChemCatChem* **2021**, *13*, 1–23.
[36] M. Bowker, P. Hellier, D. Decarolis, D. Gianolio, K. M. H. Mohammed, A. Stenner, T. Huthwelker, P. P. Wells, *Phys. Chem. Chem. Phys.* **2020**, *22*, 18911–18918.
[37] S. Tanuma, C. J. Powell, D. R. Penn, *Surf. Interf. Anal.* **1991**, *17*, 911.
[38] M. A. Flores-Mancera, J. S. Villarrubia, G. Massillon-JL, *ACS Omega* **2020**, *5*, 4139–4147.
[39] R. A. Rymzhanov, N. A. Medvedev, A. E. Volkov, *Nuclear Instruments and Methods in Physics Research B* **2015**, *354*, 292–296. https://xpsdatabase.com/quantitation-rsfs-and-atom-results/.

Manuscript received: November 15, 2023
Revised manuscript received: January 19, 2024
Accepted manuscript online: January 29, 2024
Version of record online: February 21, 2024